Regular Articles

Faustyn Recha*, Katarzyna Łuczak, Mateusz Jan Jędrzejko and Tomasz Krykowski

Functions of changes in the mechanical properties of reinforcing steel under corrosive conditions

https://doi.org/10.1515/eng-2025-0150
Received June 27, 2025; accepted November 3, 2025;
published online December 31, 2025

Abstract: Corrosion of internal steel reinforcement is one of the main reasons causing reinforced concrete (RC) structure degradation. In order to safely use and extend the durability of the structure, it is important to understand the corrosion mechanism of steel and its influence on the RC structure. Presented research in this article covers a study on the durability of reinforcing steel in strong aggressive environments condition, induced by different concentrations of chloride ions. The main aim of the research was to determine the course of changes in the mechanical properties of reinforcing steel exposed to different environmental conditions as well as its treatments (i.e., simulate the concrete cover). A current experimental investigation was carried out for reinforcing steel with an initial yield strength of 500 MPa, as such steel is currently commonly used in RC structures. The study demonstrated that changes in steel bar parameters depended on the concentration of the aggressive agent (Cl^- ions) and the presence of concrete cover. The largest changes in yield strength (over 28 %) and reduction in tensile strength (over 32 %) were obtained in an environment with a 6 % NaCl concentration for samples without concrete cover. For the same environment, a reduction in Young's modulus of over 10 % of the initial value was observed. Furthermore, functions representing the relationship between the concentration of chloride ions on the surface of the tested reinforcement samples and the mechanical parameters of the steel were evaluated. The presented empirical functions are an original element of this article, not published so far. Thanks to this, it is possible to estimate changes in the properties of reinforcing steel based on the reading of chloride ion concentration in RC structures. Additionally, the structure of the material subject to corrosion processes was analyzed using scanning electron microscopy (SEM) to assess the degradation and corrosion progress of tested steel bars. The obtained experimental results highlighted the corrosion influence of steel bars for RC structures.

Keywords: corrosion reinforced; steel parameters; degradation of RC; durability of RC; yielding strength; elastic modulus

***Corresponding author: Faustyn Recha**, Faculty of Architecture, Civil Engineering and Applied Arts, Academy of Silesia, 40-555, Rolna Street 43, Katowice, Poland, E-mail: faustyn.recha@wst.pl. https://orcid.org/0000-0002-8720-3382
Katarzyna Łuczak, Faculty of Architecture, Civil Engineering and Applied Arts, Academy of Silesia, 40-555, Rolna Street 43, Katowice, Poland, E-mail: katarzyna.łuczak@wst.com.pl
Mateusz Jan Jędrzejko, School of Civil and Hydraulic Engineering, Huazhong University of Science and Technology, Wuhan, China, E-mail: jedrzejko@hust.edu.cn
Tomasz Krykowski, Faculty of Civil Engineering, Department of Mechanics and Bridges, Silesian University of Technology, Akademicka Street 5, 44-100, Gliwice, Poland, E-mail: tomasz.krykowski@polsl.pl. https://orcid.org/0000-0002-7294-1788

Nomenclature

$m_{0,i}$	initial mass of rebar
m_t	final mass of rebar
Δm	mass loss
Δm_{avg}	average mass loss
Δm_p	percentage mass loss
α_{corr}	corrosion degree
P	ultimate force
σ	ultimate stress
$\overline{\sigma}$	average ultimate stress
f_y	yielding strength
$f_{y,avg}$	average yielding strength
$\Delta f_{y,avg}$	average differences of yielding strength between specimens investigated in control and tested environments
$\overline{\Delta f}_{y,avg}$	percentage difference of $\Delta f_{y,avg}$
f_m	ultimate strength
$f_{m,avg}$	average ultimate strength
$\Delta f_{m,avg}$	average differences of ultimate strength between specimens investigated in control and tested environments
$\overline{\Delta f}_{m,avg}$	percentage difference of $\Delta f_{m,avg}$
ε_y	yielding strains
$\varepsilon_{y,avg}$	average yielding strains
$\Delta\varepsilon_{y,avg}$	average differences of yielding strains between specimens investigated in control and tested environments
$\overline{\Delta\varepsilon}_{m,avg}$	percentage difference of $\Delta\varepsilon_{y,avg}$.
E_s	elastic module
$E_{s,avg}$	average elastic module

$\Delta E_{s,avg}$	average differences of elastic module between specimens investigated in control and tested environments
$\overline{\Delta E}_{s,avg}$	percentage difference of $\Delta E_{s,avg,i}$.
$k_{y,3}$	steel yield strength ratios of samples without and with concrete cover for a concentration of 3 % chloride ions
$k_{y,6}$	steel yield strength ratios of samples without and with concrete cover for a concentration of 6 % chloride ions
$k_{m,3}$	steel ultimate strength ratios of samples without and with concrete cover for a concentration of 3 % chloride ions
$k_{m,6}$	steel ultimate strength ratios of samples without and with concrete cover for a concentration of 6 % chloride ions
c_{Cl}	concentration of chloride ions
x_i	i-th value of variable x (e.g. for f_y, f_m, ε_y)

1 Introduction

The problems of corrosion caused by the release of chloride ions into the concrete cover of reinforced concrete (RC) structures are the subject of many publications [1–6], and scientific monographs [7, 8]. The effect of the chloride-induced corrosion process for case the steel reinforcement, apart from the degradation of the reinforcing bars affecting the load-bearing capacity of the structural elements, is also cracking of the concrete cover [9–13] which leads to the reduction of adhesion at the interface of steel-concrete [14–17] and degradation of the basic mechanical parameters of steel bars itself [18–22]. RC structures affected by the corrosion of the internal steel reinforcement are subjected to the decrease of designed load-bearing capacity which influences the durability of the structural elements [23, 24], as well as leads to abnormal deflections [25–28]. Additionally, corrosion of internal steel reinforcement significantly increases the maintenance cost of the structure [29, 30].

Among available research on the assessment of the chloride impact on the mechanical parameters of steel, studies conducted by Moreno et al. [20] and Zhu et al. [31] provide important insights on reducing the yield strength of steel caused by chloride corrosion. Moreno et al. [20] in his research, presented the formulation of a mathematical model, describing the relationship between the mechanical properties of certain corrosion of steel and its reduction in bar diameter. While Zhu et al. [31] article presents a detailed analysis of the impact of the corrosion degree and its morphology in terms of the long corrosion exposure process, reaching 26–28 years. Both works are based on the analysis of the degree of corrosion represented by the loss of reinforcement mass, which is problematic when analyzing existing structures without invasive tests. The methodology proposed in this paper is based on the dependencies of changes in the mechanical parameters of steel as a function of the concentration of chloride ions in concrete and in corroded areas, the measurement of which is a much simpler test.

Analyzing the available publications, it can be noticed that a relatively small group of research [32, 33]concerns the assessment of the chloride ions influence on the evolution of the elastic modulus as a function of the intensity of corrosion processes and time. The research in this field presented in [32] was performed for steel with an initial yield strength not exceeding 400 MPa. Currently, steels with higher material parameters are commonly used in RC structures, which indicates the need to conduct further investigation for steel with an initial yield strength of 500 MPa and higher.

Based on the above background, current work presents extensive research on the impact of an aggressive environment characterized by variable chloride ion concentration on the evolution of the mechanical properties of reinforcing steel. The tests were performed for reinforcing steel with an initial yield strength of 500 MPa (currently commonly used in RC structures), which fulfills the current knowledge gaps in this field. Furthermore, this research presents the formulation of analytical relationships between the concentration of chloride ions on the surface of the tested reinforcement samples and the mechanical properties of the steel. As part of the research carried out, scanning electron microscopy (SEM) allowed to evaluate the surfaces properties of tested samples on which corrosion processes were forced. Conducted analyses were carried out by comparing the results obtained for analogous specimens of reinforcing bars performed in a neutral (i.e., control) environment.

2 Experimental tests program

The test program consisted of 23 ribbed steel bars made of B500SP steel, which the chemical composition is given in Table 1. The nominal diameter of samples was Ø8 mm and its a length of 200 mm (scenarios A-D) and 250 mm (scenarios E and F). Six different variants of environmental impact were adopted in the current study. Series A serves as a control group corresponding to the air-dry conditions and consists of three rebars. The air-dry samples were stored in laboratory conditions (inside a closed room) where they had no access to external conditions. Under these conditions, the impact of corrosion was assumed to be negligible, so no changes were noted in Table 2. Another four bars were immersed in tap water (scenario B), and the next two series of four bars each were immersed in a solution of 3 % and 6 % sodium chloride NaCl, respectively (scenarios C and D). The last two series were embedded in concrete (i.e., to simulate concrete cover) to which an aqueous solution of chloride ions Cl^- was added at the stage of preparing the concrete

Table 1: Chemical composition of B500SP reinforcing steel as declared by the manufacturer.

Assay	Maximum content of elements (%)							$C_{eq.max}$ (%)
	C	Mn	Si	P	S	Cu	N	
Steel smelting	0.220	1,600	0.550	0.050	0.050	0.800	0.012	0.500
Finished product	0.240	1,650	0.600	0.055	0.055	0.850	0.013	0.520

C – carbon, Mn – manganese, Si – silicon, P – phosphorus, S – sulfur, Cu – copper, *N* – nitrogen, $C_{eq.max}$ – carbon equivalent, according to [1].

Table 2: Summary of tested samples, treatments, and gravimetric results.

Scenario	Treatment condition	Sample	$m_{0,i}$ (g)	$m_{t,i}$ (g)	Δm_i (g)	S_i (–)	$\Delta m_{avg,i}$ (g)	$\Delta m_{p,i}$ (%)	$\alpha_{corr,i}$ (%)
A	Air-dry (control)	P_1	77.13	77.13	0.00	0.000	0.00	0.00	0.00
		P_2	78.36	78.36	0.00			0.00	
		P_3	78.66	78.66	0.00			0.00	
B	Tap water	P_4	77.76	76.29	1.47	0.4187	1.04	1.89	1.33
		P_5	77.74	76.77	0.97			1.25	
		P_6	79.62	78.29	1.33			1.68	
		P_7	78.11	77.72	0.39			0.50	
C	3 % NaCl water solution	P_8	78.05	76.70	1.35	0.1565	1.24	1.73	1.61
		P_9	77.39	76.38	1.01			1.30	
		P_{10}	75.20	73.79	1.41			1.88	
		P_{11}	76.24	75.06	1.18			1.55	
D	6 % NaCl water solution	P_{12}	78.12	76.89	1.23	0.2765	1.54	1.58	1.96
		P_{13}	77.70	76.13	1.57			2.0	
		P_{14}	79.05	77.67	1.38			1.75	
		P_{15}	79.13	77.16	1.97			2.49	
E	Concrete cover and 3 % NaCl water solution	P_{16}	97.56	96.96	0.60	0.1194	0.74	0.61	0.76
		P_{17}	96.71	96.01	0.70			0.73	
		P_{18}	96.19	95.26	0.93			0.97	
		P_{19}	98.00	97.26	0.74			0.75	
F	Concrete cover and 6 % NaCl water solution	P_{20}	99.13	98.00	1.13	0.1600	1.30	1.14	1.34
		P_{21}	98.38	97.19	1.19			1.21	
		P_{22}	97.14	95.60	1.54			1.58	
		P_{23}	95.52	94.15	1.37			1.43	

$m_{0,i}$ is the initial mass of rebar; $m_{t,i}$ is final mass of rebar; Δm_i is mass loss; s_i is population standard deviation $\Delta m_{avg,i}$ is average mass loss; $\Delta m_{p,i}$ is percentage mass loss; $\alpha_{corr,i}$ – corrosion degree.

mixture, also with a concentration of 3 % and 6 %, respectively (scenarios E and F). These samples were encased in concrete with a diameter of approximately 60 mm, thus ensuring a reinforcement cover of approximately 25 mm. The concrete section covered the center of the reinforcing bars at a length of 80 mm, as presented in Figure 1. The proposed method of simulating the corrosion process was aimed at maximally reflecting the course of natural corrosion, and in the case of samples E and F, omitting the time necessary for chloride ion dissipation. A detailed summary of the test samples with the gravimetric analysis results for all variants of environmental aggression are presented in Table 2.

$$C_{eq.\ max} = C + \frac{Mn}{6} + \frac{(Cr + V + Mo)}{5} + \frac{(Cu + Ni)}{15} \quad (1)$$

The concrete used in this study were made with sand of fraction 0–2 mm, washed aggregate with granulation of 2–8 mm, and Portland cement CEM I, 42.5 *N*. The concrete was mixed with the ratio of 0.54/1.00/1.23/4.92, corresponding to water/cement/sand/aggregate. Table 3 summaries the properties of concrete used as a cover for steel bars in scenarios E and F. Based on the Eurocode standard [34], the used concrete can be classified as C40/50. For each research variant, four identical samples were prepared and then subjected to uniaxial compression in the Cyber-Plus Evolution testing machine. After 24 h from casting the concrete, samples of E

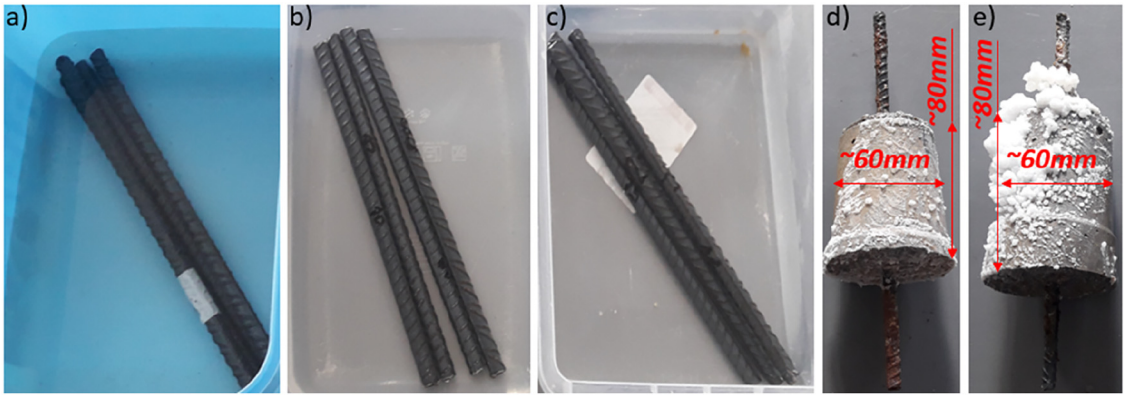

Figure 1: Samples before testing: a) Scenario B, b) scenario C, c) scenario D; after testing: d) Scenario E, e) scenario F).

Table 3: Mechanical properties of concrete used as a cover for steel rebars.

Scenario	Sample	Dimension (mm)	P_i (kN)	σ_i (MPa)	$\overline{\sigma_i}$ (MPa)
E (3 % NaCl)	$C_{E,1}$	150 × 150	1143.43	50.82	51.40
	$C_{E,2}$		1140.63	50.69	
	$C_{E,3}$		1191.91	52.97	
	$C_{E,4}$		1150.02	51.11	
F (6 % NaCl)	$C_{F,1}$	150 × 150	1182.56	52.56	51.05
	$C_{F,2}$		1153.02	51.25	
	$C_{F,3}$		1088.27	48.37	
	$C_{F,4}$		1170.36	52.02	

P_i is the ultimate force; σ_i is ultimate stress; $\overline{\sigma_i}$ is the average ultimate stress.

and F scenarios were placed in the same solutions of chloride ions concentrations as during the preparation of the concrete mixture, thus the chloride ions were not extracted. All concrete specimens were cured over 28 days before any testing was conducted.

The total duration of presented study for all variants was 12 months. After this time, the samples were removed from the solutions (scenarios B, C, and D), the concrete covers were split (in the case of scenarios E and F) and a gravimetric analysis was performed again, separately for each bar. The weight loss of the bars was determined based on the difference between the initial mass m_0 and the mass m_t weighed after de-rusting the bars in phosphoric acid and mechanical cleaning. The difference in Δm measurements was the actual loss of reinforcement mass (Eq. (2)), which was also converted into a percentage loss of Δm_p and the degree of corrosion α_{corr}, based on the following equations accordingly [3, 4]:

$$\Delta m_i = m_{0,i} - m_{t,i} \tag{2}$$

$$\Delta m_{p,i} = \frac{m_{0,i} - m_{t,i}}{m_{0,i}} \cdot 100\% \tag{3}$$

$$\alpha_{corr.i} = \frac{\Delta m_{avg.i}}{m_{0.avg.i}} \cdot 100\% \tag{4}$$

where Δm_i is a real loss of reinforcement mass, $\Delta m_{p,i}$ is the percentage loss of reinforcement mass, $m_{0,i}$ is the initial mass (before starting the test), $m_{t,i}$ is the final mass (after the test), $\Delta m_{avg,i}$ is the ratio of the average loss of reinforcement mass for each tested environment to the average initial mass in the analyzed environment $m_{0,avg,i}$.

The corroded bars from different scenarios were subjected to a static tensile test in a Quasar testing machine under laboratory conditions. After curing in a salt solution, the concrete cover was split (scenario E and F) and only the sections within the concrete cover were tested. The remaining reinforcement was cut off before testing in a tensile testing machine. Figure 2 presents the corroded bars and testing machine.

Based on the conducted static tensile tests of reinforcing steel samples, the results of the actual yield strength $f_{y,i}$, ultimate tensile strength $f_{m,i}$ and strain (measured through strain gauges attached to rebar) at the moment of yielding $\varepsilon_{y,i}$ were obtained separately for each tested sample. Measurements of individual sample elongations, which served as the basis for determining bar deformations, were automatically measured using a measuring system implemented in the testing machine. The rate of increase in crosshead elongation was adopted in accordance with Method A of the ISO 6892 standard [35], minimizing measurement uncertainty of the test results. Then, for each corrosion environment (test variants A-E), the average values of the actual yield strength $f_{y,avg}$, ultimate tensile strength $f_{m,avg}$ and strain at the moment of plasticization $\varepsilon_{y,avg}$ were determined. Exceptionally, for variant B (samples placed in tap water), the average value was determined for three samples P_4, P_5, P_7. Sample P_6 was not included, due to the significant

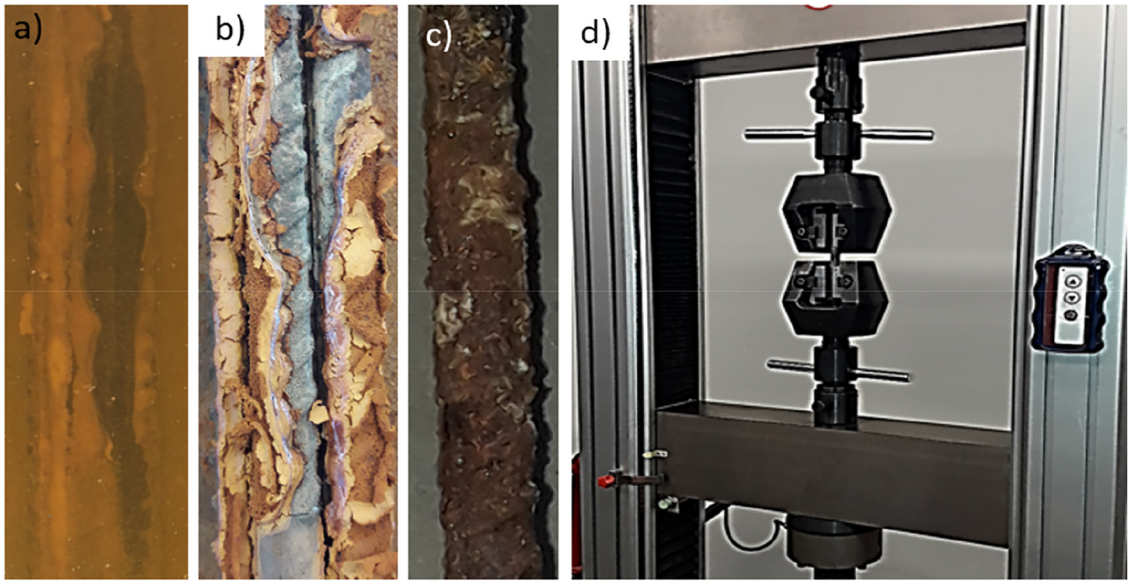

Figure 2: Stages of steel rebars during the study: a) Immersed in the solution (scenario C), b) dried out after immersion period (scenario C), c) steel rebar after removing concrete cover (scenario E) d) tensile testing machine.

deviation of this sample compared to obtained stress values from other samples in this group, which could distort the result of the entire study in this series.

The obtained average values $f_{y,avg}$, $f_{m,avg}$, $\varepsilon_{y,avg}$ for each variant of environmental aggression were compared with the average result obtained for the control samples in the absence of any corrosion aggression, respectively $f_{y,avg,A}$, $f_{m,avg,A}$, $\varepsilon_{y,avg,A}$. For comparison purposes, absolute differences of the analyzed parameters (i.e., $\Delta f_{y,avg,i}$, $\Delta f_{m,avg,i}$, $\Delta\varepsilon_{y,avg,i}$) were determined based on the following equations [5–7]:

$$\Delta f_{y,\,avg,\,i} = f_{y,\,avg,\,i} - f_{y,\,avg,\,A} \tag{5}$$

$$\Delta f_{m,\,avg,\,i} = f_{m,\,avg,\,i} - f_{m,\,avg,\,A} \tag{6}$$

$$\Delta\varepsilon_{y,\,avg,\,i} = \varepsilon_{y,\,avg,\,i} - \varepsilon_{y,\,avg,\,A} \tag{7}$$

The percentage share of the resulting changes $\overline{\Delta f}_{y,\,avg,\,i}$, $\overline{\Delta f}_{m,\,avg,\,i}$, $\overline{\Delta\varepsilon}_{y,\,avg,\,i}$ in relation to the base values $f_{y,avg,A}$, $f_{m,avg,A}$, $\varepsilon_{y,avg,A}$, accordingly in equations [8–10]:

$$\overline{\Delta f}_{y,\,avg,\,i} = \frac{\Delta f_{y,\,avg,\,i}}{f_{y,\,avg,\,A}} \times 100\% \tag{8}$$

$$\overline{\Delta f}_{m,\,avg,\,\mathrm{i}} = \frac{\Delta f_{m,\,avg,\,i}}{f_{m,\,avg,\,A}} \times 100\% \tag{9}$$

$$\overline{\Delta\varepsilon}_{m,\,avg,\,\mathrm{i}} = \frac{\Delta\varepsilon_{m,\,avg,\,i}}{\varepsilon_{m,\,avg,\,A}} \times 100\% \tag{10}$$

Table 4 detailed summarized the test result for each tested bar, with the minus (–) sign corresponding to a decrease in a given parameter, and the plus (+) sign corresponding to its increase.

Recorded stress and corresponding strain measurements during the tensile tests on corroded samples allowed for the generation of stress-strain (σi – εi) graphs for each tested sample. Figures 3 and 4 present stress-strain graphs for each steel bar in groups A, B, C, and D, E, and F, respectively. In most cases, very similar, nearly identical stress values were obtained for the individual test scenarios, confirming the accuracy of the conducted study. The assumed initial values oscillated around 150 MPa and were referred to the strain at a stress of 450 MPa. In individual cases, other values were selected to be appropriate for the elastic range. By knowing the adequate stress-strain relationship, it was possible to determine the actual elastic modulus ($E_{s.i}$), as the ratio of differences in stresses $\Delta\sigma_{21.i}$ and corresponding strains $\Delta\varepsilon_{21.i}$ from the elastic part of table 4 (Eq. (11)):

$$E_{s.i} = \frac{\Delta\sigma_{21.i}}{\Delta\varepsilon_{21.i}} = \frac{\sigma_{2.i} - \sigma_{1.i}}{\varepsilon_{2.i} - \varepsilon_{1.i}} \tag{11}$$

where $\sigma_{1.i}$,$\sigma_{2.i}$ and $\varepsilon_{1.i}$,$\varepsilon_{2.i}$ are the values of stresses and strains representative of the elastic phase, respectively. Figure 5 graphically represents the concept of evaluating the elastic modulus from conducted tensile tests.

Same as in the case of the bar's yielding/ultimate strength, the average values of elastic modulus $E_{s,avg}$ was

Table 4: Yielding, ultimate strengths, and corresponding strains of all tested samples.

Scenario	Treatment condition	Sample	$f_{y,i}$ (MPa)	$f_{y,avg}$ (MPa)	$\Delta f_{y,avg}$ (MPa)	$\overline{\Delta f}_{y,avg}$ (%)	$f_{m,i}$ (MPa)	$f_{m,avg}$ (MPa)	$\Delta f_{m,avg}$ (MPa)	$\overline{\Delta f}_{m,avg}$ (%)	$\varepsilon_{y,i}$ (10^{-3})	$\varepsilon_{y,avg}$ (10^{-3})	$\Delta\varepsilon_{y,avg}$ (10^{-3})	$\overline{\Delta\varepsilon}_{m,avg}$ (%)
A	Air-dry (control)	P_1	550.65	540.52	0.00	0.00	638.93	617.54	0.00	0.00	3.40	3.17	0.00	0.00
		P_2	532.64				605.13				3.00			
		P_3	538.26				608.56				3.10			
B	Tap water	P_4	521.89	517.26	−23.26	−4.30	621.22	614.24	−3.30	−0.53	3.10	2.90	−0.27	−8.52
		P_5	517.12				618.00				2.80			
		P_6	352.61				446.28				1.10			
		P_7	512.77				603.50				2.80			
C	3 % NaCl water solution	P_8	508.34	485.49	−55.03	−10.18	503.34	499.37	−118.17	−19.14	3.10	2.75	−0.42	−13.25
		P_9	513.82				512.79				2.80			
		P_{10}	398.14				461.92				2.50			
		P_{11}	521.67				519.43				2.60			
D	6 % NaCl water solution	P_{12}	392.16	385.76	−154.76	−28.63	472.55	419.56	−197.98	−32.06	1.80	2.13	−1.04	−32.81
		P_{13}	341.86				332.11				1.80			
		P_{14}	346.24				389.63				1.70			
		P_{15}	462.76				483.96				3.20			
E	Concrete and 3 % NaCl solution	P_{16}	517.67	519.95	−20.57	−3.81	550.18	584.62	−32.92	−5.33	3.20	3.23	0.60	1.89
		P_{17}	515.31				548.93				3.00			
		P_{18}	468.15				591.54				3.40			
		P_{19}	578.66				647.82				3.30			
F	Concrete and 6 % NaCl solution	P_{20}	503.10	500.19	−40.33	−7.46	593.47	572.83	−44.71	−7.24	3.40	3.58	0.41	12.93
		P_{21}	508.62				591.32				3.60			
		P_{22}	499.63				568.24				3.80			
		P_{23}	489.39				538.29				3.50			

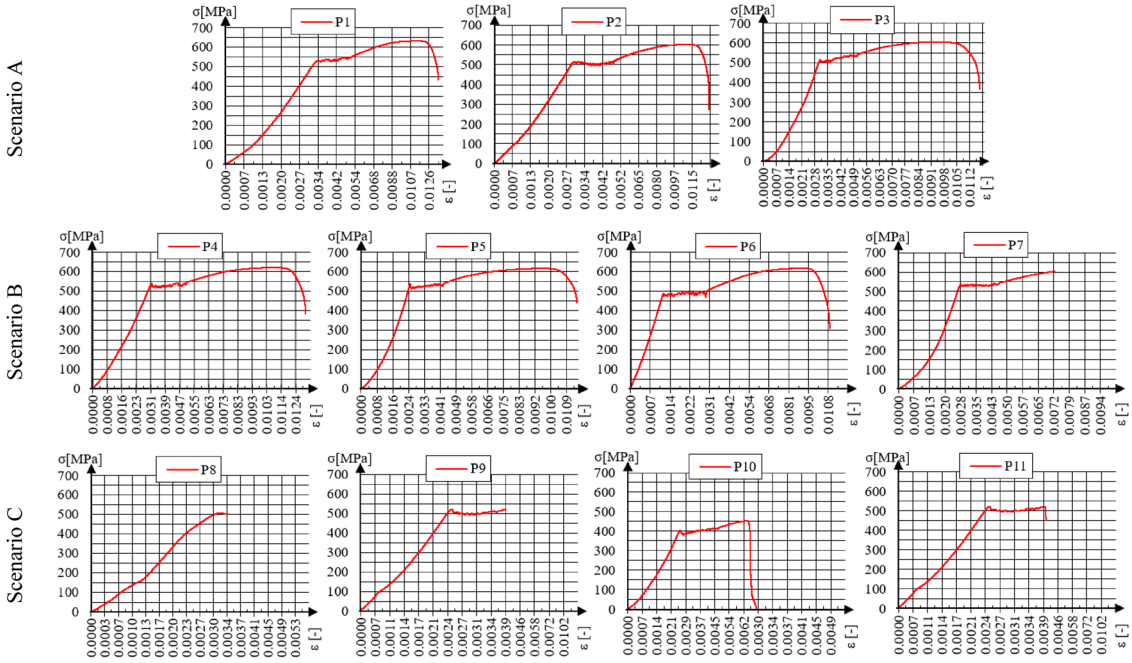

Figure 3: Stress-strains relationships for testes samples – scenarios A, B, C.

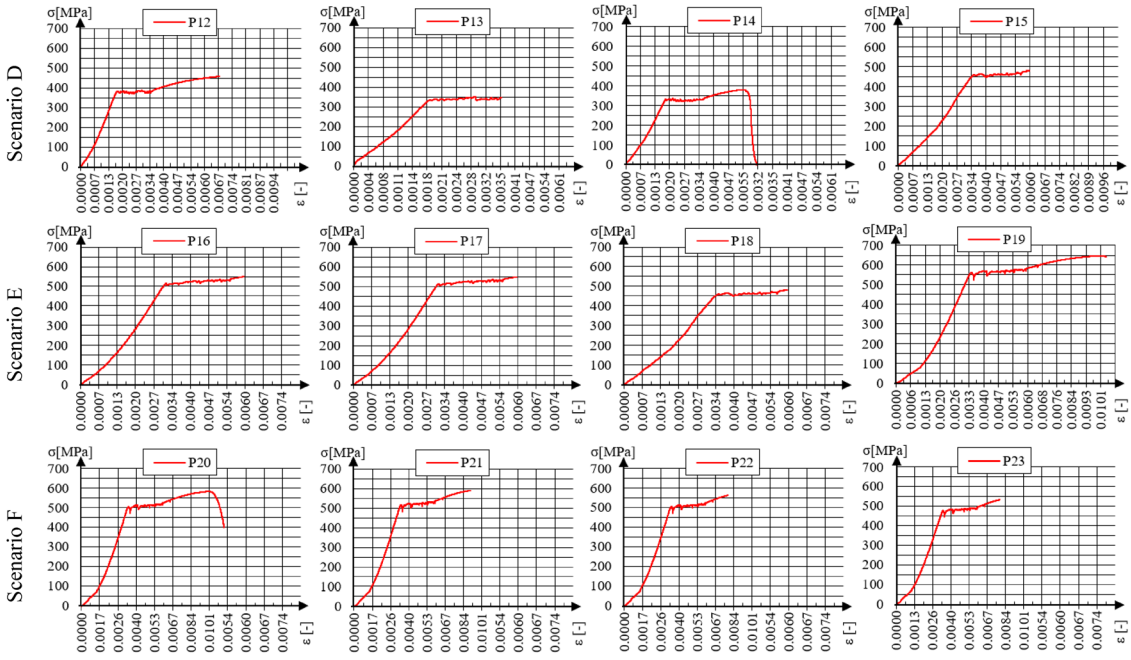

Figure 4: Stress-strains relationships for all tested samples – scenarios D, E, F.

determined separately for each bar of every scenario. Furthermore, the change in the average elastic modulus for different scenarios (i.e., environmental conditions), represented by the absolute value ($\Delta E_{s,avg,i}$), were determined by the difference between the average elastic modulus of control scenario A (i.e., air-dry condition) and the average elastic modulus of the corresponding group according to the equation [12]:

$$\Delta E_{s,avg,i} = E_{s,avg,A} - E_{s,avg,i} \tag{12}$$

Then, the percentage decrease in the elastic modulus $\overline{\Delta E}_{s,avg,i}$ relative to the base value was evaluated, which was

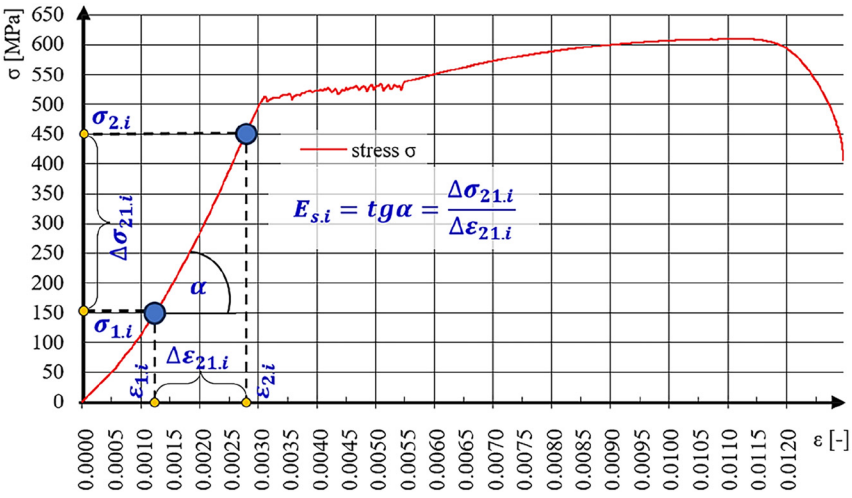

Figure 5: Schematic procedure for obtaining the elastic modulus of tested steel bars on the example of sample P_1.

determined as the ratio of the average decrease in the elastic modulus $\Delta E_{s,avg,i}$ and the control value $E_{s,avg,A}$ represented by treatment scenario A (Eq. (13)):

$$\overline{\Delta E}_{s,\,avg,\,i} = \frac{\Delta E_{s,\,avg.\,i}}{E_{s,\,avg,\,A}} \times 100\% \tag{13}$$

The same analogy of labeling as in case of yielding/ultimate tensile strength was applied to the analysis of elastic modulus results, which assumed that the minus (–) sign corresponds to a decrease in the parameter and at the same time no positive results were obtained that would indicate an increase in the analyzed parameter. As a consequence of the unrepresentative result of the tensile strength test, sample P_6 was also rejected (more than 65 % deviation from the average of the remaining results in the B scenario studies). A list of representative values defining the elastic range of the tested samples in accordance with the equation [11] and the values of the reduced elastic modulus obtained for each variant of environmental aggression are summarized in Table 5.

Table 5: Stresses, corresponding strains, and elastic modulus of all tested samples.

Treatment condition	Sample	$\sigma_{1,i}$ (MPa)	$\sigma_{2,i}$ (MPa)	$\varepsilon_{1,i}$ (10^{-3})	$\varepsilon_{2,i}$ (10^{-3})	$\Delta\sigma_{,i}$ (MPa)	$\Delta\varepsilon_{,i}$ (10^{-3})	$E_{s,i}$ (GPa)	$E_{s,avg,i}$ (GPa)	$\Delta E_{s,avg,i}$ (GPa)	$\overline{\Delta E}_{s,\,avg,\,i}$ (%)
Air-dry (control)	P_1	149.54	500.34	1.39	3.13	350.80	1.74	201.91	202.89	0.00	0.00
	P_2	150.04	500.77	1.11	2.86	350.74	1.75	200.02			
	P_3	150.66	500.91	1.35	3.04	350.25	1.69	206.75			
Tap water	P_4	150.76	499.59	1.14	2.97	348.83	1.83	190.96	195.17	−7.72	−3.81
	P_5	149.40	499.18	1.04	2.81	349.78	1.78	196.70			
	P_6	149.40	300.65	0.54	1.00	151.25	0.46	326.91			
	P_7	150.70	501.24	1.12	2.90	350.54	1.77	197.85			
3 % NaCl water solution	P_8	149.93	500.12	1.13	3.04	350.20	1.92	182.77	187.30	−15.60	−7.69
	P_9	150.10	500.86	1.10	2.91	350.76	1.81	194.11			
	P_{10}	150.89	350.74	1.23	2.34	199.84	1.11	180.36			
	P_{11}	149.76	501.02	1.18	3.01	351.26	1.83	191.95			
6 % NaCl water solution	P_{12}	150.87	349.55	0.84	1.87	198.69	1.03	192.95	181.05	−21.85	−10.77
	P_{13}	150.32	300.15	0.95	1.75	149.84	0.80	187.44			
	P_{14}	149.95	300.83	0.98	1.78	150.88	0.80	188.18			
	P_{15}	150.29	400.55	1.41	3.02	250.26	1.61	155.61			
Concrete and 3 % NaCl solution	P_{16}	150.62	499.83	1.26	3.04	349.21	2.00	195.65	192.57	−10.32	−5.09
	P_{17}	149.87	500.23	1.32	3.12	350.36	2.00	194.64			
	P_{18}	149.32	499.16	1.36	3.24	349.84	2.00	186.09			
	P_{19}	150.75	501.99	1.43	3.24	351.25	2.00	193.91			
Concrete and 6 % NaCl solution	P_{20}	299.42	501.99	2.14	3.18	202.58	1.00	193.50	184.74	−18.16	−8.95
	P_{21}	150.20	501.21	1.40	3.26	351.01	2.00	188.26			
	P_{22}	149.85	499.36	1.31	3.28	349.51	2.00	177.42			
	P_{23}	149.66	500.21	1.31	3.26	350.55	2.00	179.77			

$\sigma_{1,i}$, $\sigma_{2,i}$ – stresses at two consecutive reference points; $\varepsilon_{1,i}$, $\varepsilon_{2,i}$ – strains at two consecutive reference points. $\Delta\sigma_{,i}$ – increment's stress, $\Delta\varepsilon_{,i}$ – increment's strains, $E_{s,i}$ – Young's module, $E_{s,avg,i}$ – average Young's module, $\Delta E_{s,avg,i}$ – average differences of Young's module between specimens investigated in control and tested environments, $\overline{\Delta E}_{s,\,avg,i}$ – percentage difference of $\Delta E_{s,avg,i}$.

3 Microscopic analysis

To accurately assess damage caused by chloride ions, the side surfaces of corroded test specimens placed in aggressive environments were subjected to structural analysis. Observations of the surfaces of the elements were carried out using a scanning electron microscope (SEM). Structural observations confirmed the presence of damage on the steel surface exposed to the direct action of chloride ions Cl^-. Figure 6 clearly shows the surface damage of several hundred μm, around which corrosion products were accumulated in the form of a mixture of iron chlorides $FeCl_2$ and hydroxides $Fe(OH)_2$ and $Fe(OH)_3$. Moreover, there were small micro-damages and larger pits on the bar's surface, as shown in Figure 7. These damages are particularly visible in a solution with a higher concentration of chloride ions simulated with an aqueous solution of 6 % sodium chloride NaCl (series F). These pits are local and concentrated in single places. The propagation of damage and the resulting corrosion pits take the form of oval depressions and are arranged along the reinforcement axis, which confirms the analyses presented in the work [36].

During the scanning analysis, local clusters of small damages to the passive layer were found in the vicinity of the steel ribs. This is related to the higher concentration of chloride ions in this area, which results in the accumulation of damage as shown in Figure 8. The local accumulation of chloride ions Cl^- causes damage to the passive layer of iron trioxide γ-Fe_2O_3 and their migration deep into the material structure. The morphology of the steel surface made using the Back Scattered Electron (BSE) signal technique is shown in Figure 9. Chloride ions Cl^- are visible, breaking the continuity of the passive layer and penetrating into it, causing individual damage to the iron particles.

4 Parameters' evolution of steel B500SP

Changes in elastic modulus strongly depend on the impact and intensity of external environment aggression. For the samples that remained in the neutral state, the average elastic modulus was determined to be 202.89 GPa. In the case of samples immersed only in clean tap water, an average elastic modulus of 195.17 GPa was obtained (a decrease of 3.81 % compared to the control value). For test specimens immersed in aqueous solutions of three and 6 % NaCl, a mean elastic modulus of 187.30 and 181.05 GPa were obtained, respectively, corresponding to a reduction of 7.69 and 10.77 %. For the steel bars from scenarios E and F, in which environmental aggression was simulated by placing chlorides in the concrete cover at concentrations of 3 and 6 %, the average values of elastic moduli were 192.57 and 184.74 GPa, respectively. The value of elastic modulus for those samples noted a reduction of 5.09 and 8.95 % compared to the initial value in the neutral state. All the details regarding properties of the steel bars after testing are summarized in Table 3. Based on the conducted analysis, it is observed a positive impact of concrete cover on the change in steel reinforcement parameters. For each analyzed variant of the mechanical properties, the concrete cover reduces the rate of change of a given parameter over time.

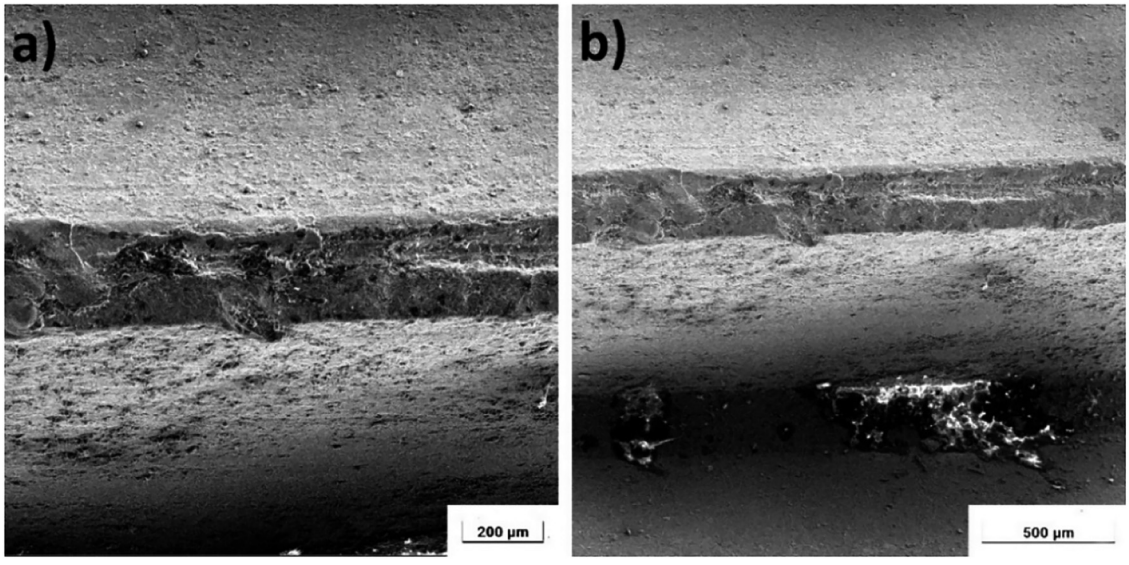

Figure 6: SEM analysis of sample P9 after immersion in 3 % NaCl solution: a) Corrosion products accumulation, b) surface defects.

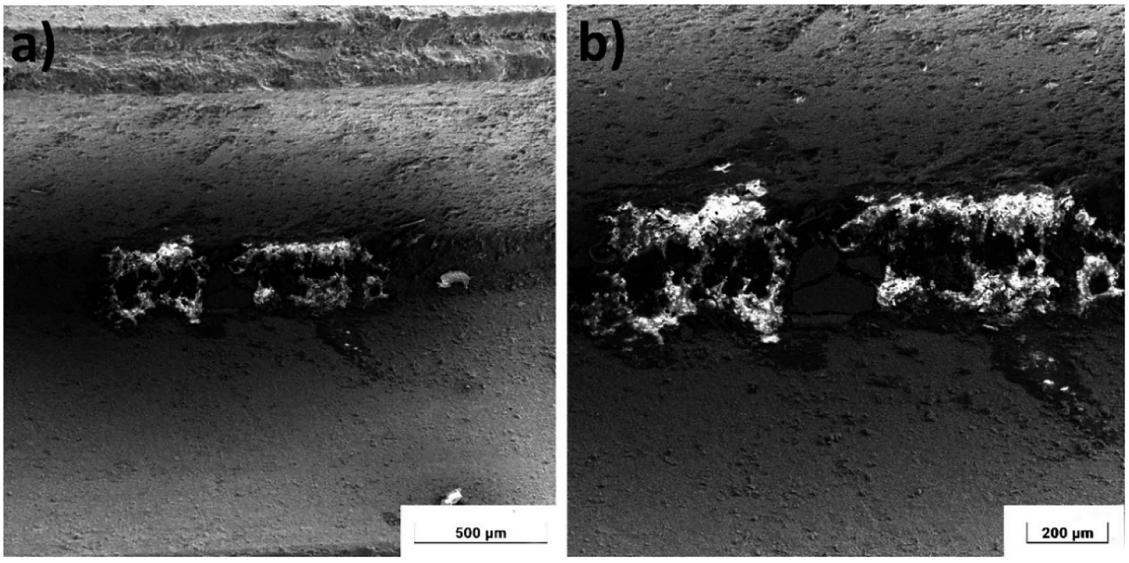

Figure 7: Corrosion pit area on the surface of rebar after immersion in 6 % NaCl solution: a) a pattern of pits along the rebar's axis at 160x magnification, b) a single corrosion pit at 300x magnification.

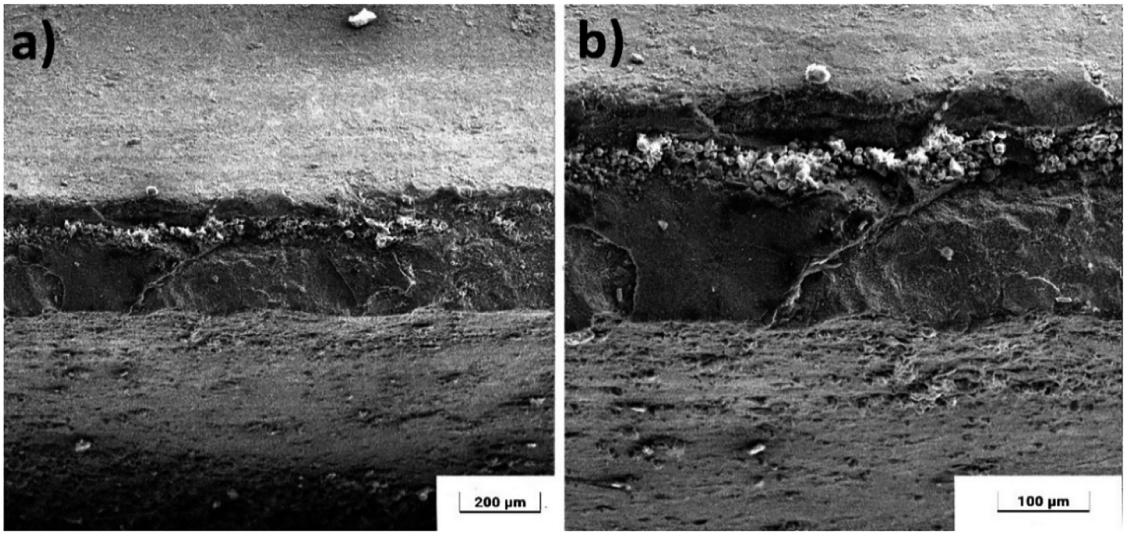

Figure 8: The surface of the rod within the ribs of steel in aqueous solutions: a) 3 % NaCl, b) 6 % NaCl.

In the case of environmental aggression simulated only by completely immersing the test samples in water, a slight decrease in the yield strength was obtained, reaching an average of 4.30 %, while the reduction in ultimate strength was almost unchanged compared to the results obtained for the control samples (0.53 % decrease). However, two remaining scenarios C and D showed a strong influence of chloride ions simulated by aqueous NaCl solutions with concentrations of 3 and 6 % on the obtained results. In the case of scenario C (3 % NaCl), the decrease in the steel yield strength was 10.18 %, while the reduction in the ultimate tensile strength of steel was reduced by 19.14 %. A similar situation was observed for 6 % NaCl concentrations, for which the reduction in the yield strength was 28.63 %, and the ultimate tensile strength was reduced by 32.06 % compared to the specimens from group A (see Table 2). Analyzing the above changes and the shape of the graphs (see Figure 5), it can be seen that increasing the concentration of chloride ions in contact with the reinforcing steel results in a decrease in the material strength/durability, which occurs after achieving the plastic stage. There is usually a situation in which the stress at the yield point is close to the stress responsible for the tensile failure of the steel. Consequently, the reinforcement does not have a

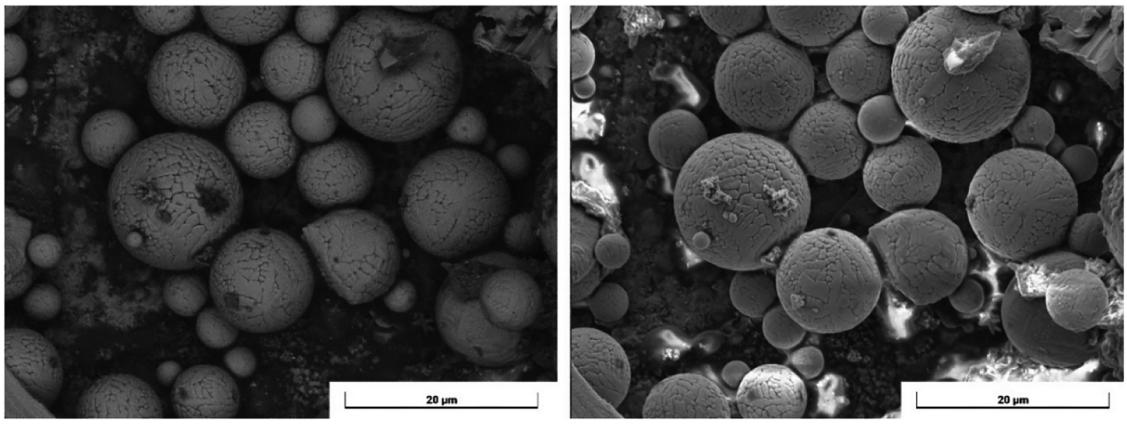

Figure 9: The structure of the rod surface at the atomic level.

plastic reserve, and the failure occurs suddenly, as a result of a brittle crack without visible narrowing.

The experimental outcome of the specimens from scenarios E and F, demonstrate a significant influence of the concrete cover on the change in the mechanical properties of steel bars subjected to a corrosive environment. In the case of samples with a concrete cover, changes in both the yield and ultimate tensile strength were analogous to those in the case of bars without a cover. A decrease in the yield strength of reinforcing steel was observed here by 3.81 % for the environmental aggression scenario E (3 % NaCl in the concrete cover) and 7.46 % for the environmental aggression simulated in scenario F (6 % NaCl in the concrete cover). The reduction in ultimate tensile strength for these variants was reduced by 5.33 and 7.24 %, respectively, compared to the initial value determined in the air-dry condition. It is worth noting that, the reduction in the mechanical properties of tested steel bars with concrete cover was proportionally smaller than that in the case of samples without cover. The concrete cover significantly impacts the mechanical behavior of steel reinforcement. This can be clearly demonstrated by comparing the ratio of yield and ultimate strength of samples without cover to those with concrete cover, under the same environment's treatments and the same chloride ion concentrations according to the equations [14–17]:

$$k_{y,3} = \frac{f_{y,avg,C}}{f_{y,avg,E}} \tag{14}$$

$$k_{y,6} = \frac{f_{y,avg,D}}{f_{y,avg,F}} \tag{15}$$

$$k_{m,3} = \frac{f_{m,avg,C}}{f_{m,avg,E}} \tag{16}$$

$$k_{m,6} = \frac{f_{m,avg,D}}{f_{m,avg,F}} \tag{17}$$

where $k_{y,3}$, $k_{y,6}$ are the ratios of the steel yield strength of samples without and with concrete cover for the environments respectively three and 6 % NaCl concentrations. Parameters $k_{m,3}$, $k_{m,6}$ are steel tensile strength ratios in samples without and with concrete cover for respectively three and 6 % concentrations of chloride ions. In the case of a concentration of 3 % chloride ions, the $k_{y,3}$ ratio reaches 2.67, while the $k_{y,6}$ increases to 3.84. Even more significant changes are observed when analyzing the ultimate tensile strength of steel. The ratio of ultimate tensile strength for samples without and with a concrete cover, $k_{m,3}$ reaches 3.59 at a 3 % NaCl concentration, and $k_{m,6}$ is 4.43 at a 6 % NaCl concentration. Therefore, it is necessary to ensure a tight concrete cover even in the event of ongoing and developing corrosion processes on the steel reinforcement surface. Based on the above analysis, it is possible to obtain the relationship between changes in the mechanical properties of reinforcement steel with electrode processes occurring on its surface, which strongly depends on the concentration of chloride ions in this area. In order to determine the functional relationships between the increase in the concentration of Cl^- ions and the evolution of individual material parameters, linear trend functions were determined showing the course of parameter changes for each analyzed environment. The trend functions are graphically presented in Figure 10.

The functions describing the course of the trend line can be directly adapted as an approximate relationship for the change of steel parameters depending on the aggression of the interacting environment. The function describing the relationships of the yield strength, ultimate strength, elastic

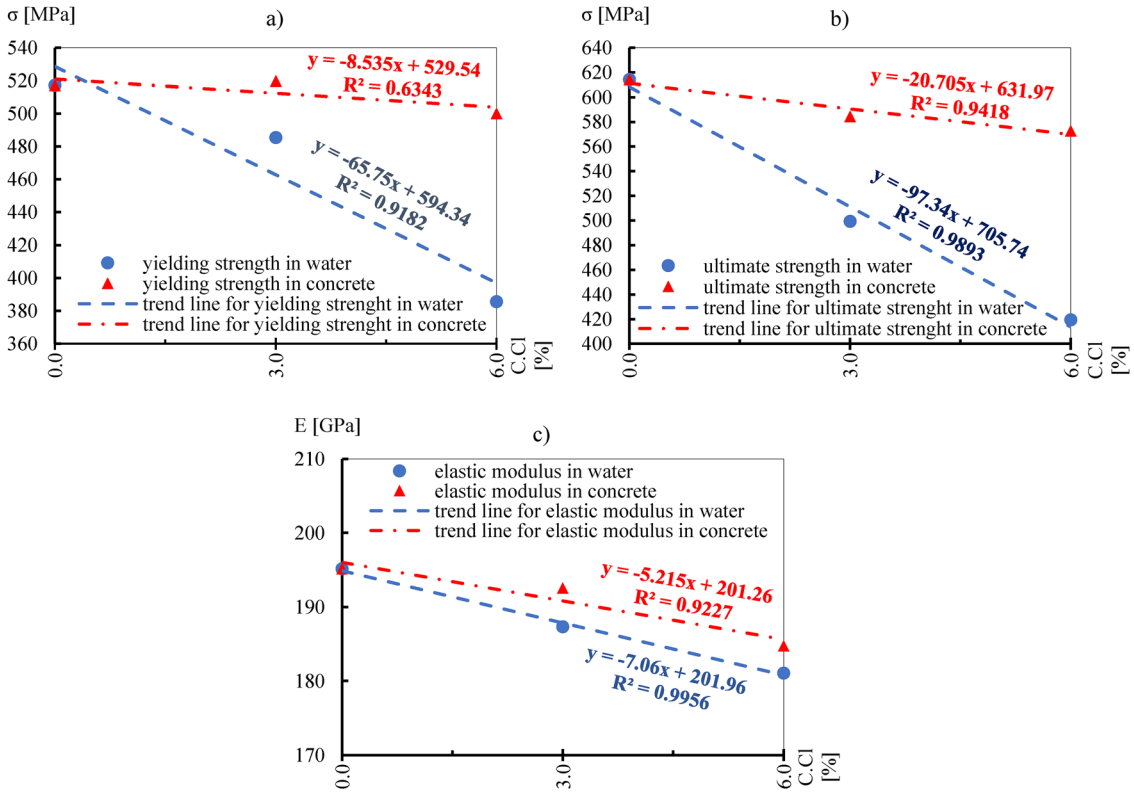

Figure 10: Graphic representation of correlations between mechanical properties of steel rebars and chloride ions for a) yielding strength, b) ultimate strength, and c) elastic modulus.

Table 6: Correlations between the mechanical properties of steel rebars and chloride ions (c_{Cl}) concentration.

Parameter	Environment	Correlation	Coefficient of determination
Yielding strength $f_{y,i}(c_{Cl})$	Concrete	$f_{y,c}(c_{Cl}) = -8.535c_{Cl}+529.54$ *MPa*	$R^2 = 0.6343$
	Water	$f_{y,w}(c_{Cl}) = -65.75c_{Cl}+594.34$ *MPa*	$R^2 = 0.9182$
Ultimate strength $f_{m,i}(c_{Cl})$	Concrete	$f_{m,c}(c_{Cl}) = -20.705c_{Cl}+631.97$ *MPa*	$R^2 = 0.9418$
	Water	$f_{m,w}(c_{Cl}) = -97.34c_{Cl}+705.74$ *MPa*	$R^2 = 0.9893$
Elastic modulus	Concrete	$E_{s,c}(c_{Cl}) = -5.215c_{Cl}+201.26$ *GPa*	$R^2 = 0.9227$
$E_{s,i}(c_{Cl})$	Water	$E_{s,w}(c_{Cl}) = -7.06c_{Cl}+201.96$ *GPa*	$R^2 = 0.9956$

modulus of the steel reinforcement, and concentrations of chloride ions are presented in Table 6.

In the relationship presented in Table 5, the concentration of c_{Cl} ions should be given as a percentage. According to the trend line graphs, these values decrease with increasing chloride ion concentration, as evidenced by the negative value of the slope coefficient of the function. For all determined functions, the coefficient of determination R^2 is greater than 0.91. The exception is the function describing the change in the yield strength of steel in the area of the concrete environment, for which this coefficient R^2 is equal to 0.63. Despite the large dispersion of the obtained results, this is the best fit of the linear function in this range. In order to compare the outcome of presented functions with the works presented in [17, 32] the above results of changes in the mechanical properties of the steel reinforcement were included as a function of the corrosion degree α_{corr}. The corrosion degree was determined based on the gravimetric analysis carried out in accordance with the equation [4]. During corrosion processes, not only does the bar lose mass, but also changes its elastic properties, represented by Young's modulus, determined based on stresses and strains,

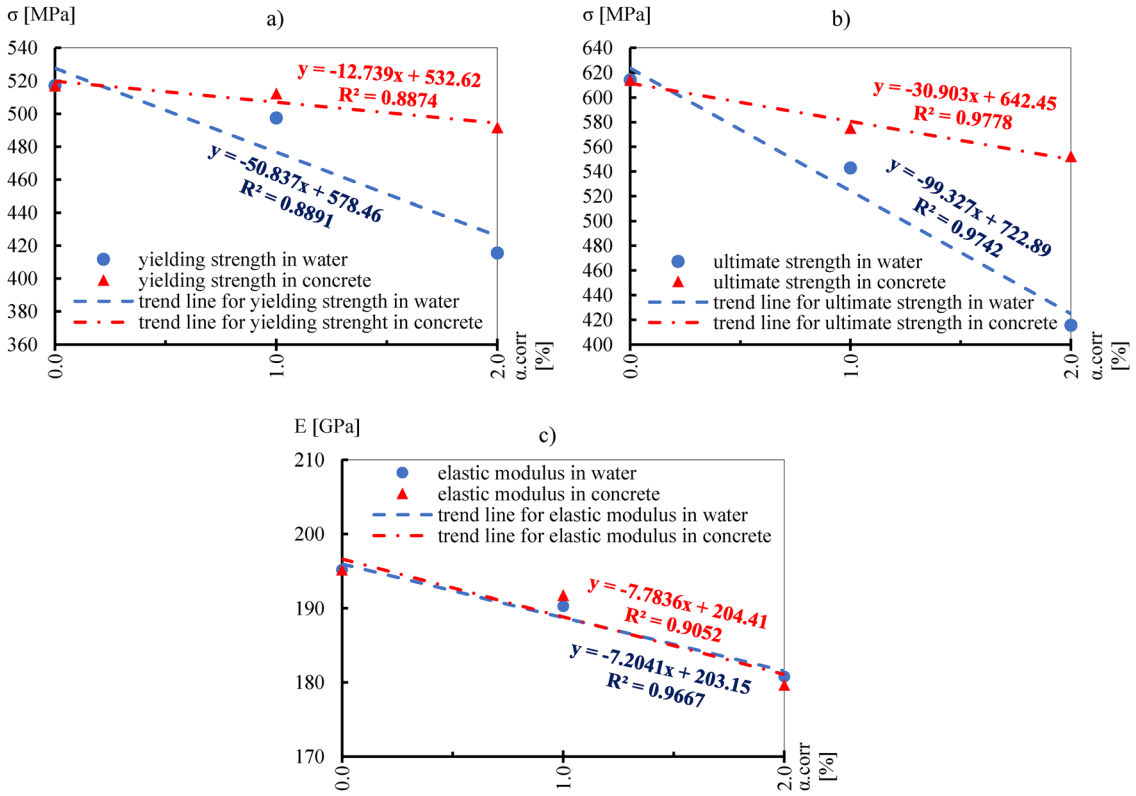

Figure 11: Graphic representation of correlations between mechanical properties of steel rebars and corrosion degree for a) yielding strength, b) ultimate strength, and c) elastic modulus.

which was the main subject of the study. Finally, these two relationships (reinforcement mass loss, represented by the α_{corr} coefficient, with physical properties) were linked and presented as linear dependence functions in the graphs in Figure 11.

Similarly to the analysis of changes in steel parameters depending on the degree of chloride ion concentration c_{Cl}, it is also possible to determine the relationship describing the process of parameter evolution as a result of the corrosion development for the generalized corrosion degree α_{corr}, as presented in Table 7.

Functions describing the changes in the steel yield strength $f_y(\alpha_{corr})$ and the steel ultimate tensile strength $f_{m.i}(\alpha_{corr})$ take forms very similar to the changes in the function of the concentration of chloride ions c_{Cl}, $f_{y.i}(c_{Cl})$ and $f_m(c_{Cl})$ respectively. Changes in the value of elastic modulus determined as a function of the generalized corrosion degree $E_{s.i}(\alpha_{corr})$ are very similar to each other regardless of the corrosion environment. It can be explained by the fact that the elastic modulus is directly influenced by corrosion aggression initiated and then propagated by Cl^- ions. To evaluate the actual corrosion degree of internal steel reinforcement, it is necessary to remove the concrete cover and then cut the rebar for the gravimetric analysis. Such measurements can significantly affect structural stability, creating a risk of collapse or permanent damage. A proper relationship between the changes in mechanical parameters of steel reinforcement and chloride ions provides estimation

Table 7: Correlations between the mechanical properties of steel rebars and corrosion degree (α_{corr})

Parameter	Environment	Correlation	Coefficient of determination
Yielding strength $f_{y.i}(\alpha_{corr})$	Concrete	$f_{y.c}(\alpha_{corr}) = -12.739\alpha_{corr}+532.62$ *MPa*	$R^2 = 0.8874$
	Water	$f_{y.w}(\alpha_{corr}) = -50.837\alpha_{corr}+578.46$ *MPa*	$R^2 = 0.8891$
Ultimate strength $f_{m.i}(\alpha_{corr})$	Concrete	$f_{m.c}(\alpha_{corr}) = -30.903\alpha_{corr}+642.45$ *MPa*	$R^2 = 0.9778$
	Water	$f_{m.w}(\alpha_{corr}) = -99.327\alpha_{corr}+722.89$ *MPa*	$R^2 = 0.9742$
Elastic modulus	Concrete	$E_{s.c}(\alpha_{corr}) = -7.7836\alpha_{corr}+204.41$ *GPa*	$R^2 = 0.9052$
$E_{s.i}(\alpha_{corr})$	Water	$E_{s.w}(\alpha_{corr}) = -7.2041\alpha_{corr}+203.15$ *GPa*	$R^2 = 0.9667$

information of the mechanical parameters of the internal steel through non-invasive tests. It could be done by measuring the chloride ions concentration within the surface of the internal steel reinforcement, without cutting the reinforcing bars. Please note that this is only an estimate procedure and it requires further investigations, including experimental verification using advanced methods.

5 Conclusions

The current study presents the investigation of five different corrosion-related environments that affected the properties of internal steel reinforcement. One environmental aggression (scenario B) was simulated by tap water, and another two (highly acidic environments), were simulated by the 3 and 6 percent sodium chloride NaCl solutions (scenarios C and D, respectively). The last two scenarios included a concrete cover environment with a simulation of full chloride ion diffusion, which was performed by adding chlorides to the mixing water of concrete to obtain concentrations of three and 6 % NaCl. Then, after appropriate preparation of all samples, a static uniaxial tensile test and microscopic analysis were performed. The obtained results were compared with the results of tensile strength of control samples that were not exposed to any environmental aggression (they remained in an air-dry state). The conducted experiments and detailed analysis of the results gave rise to the following conclusions:

- Changes in the reinforcement surface and the atomic structure of the passive layer cause local and high-intensity damage (pitting corrosion), which confirms the results obtained in the work [36]. The microscopic analysis clearly showed the degradation of the passive oxide layer on the reinforcement surface as a result of its breakdown by chloride ions which confirming the results in work [37–41]. The research confirmed that changes in the mechanical properties of the reinforcement result directly from the interaction of choride ions, which penetrate the passive layer.
- Increasing the concentration of chloride ions in contact with the reinforcing steel results in the decreasing of material durability responsible for the post-yielding behavior. There is usually a situation in which the stress level at the yield point is close to the stress corresponding to the ultimate tensile strength of the steel. The reinforcement does not have a plastic reserve, and the failure occurs suddenly, as a result of a brittle crack without visible narrowing. Corroded steel becomes brittle because the corrosion process weakens its internal structure, creating cracks and fissures, as confirmed by microscopic scanning (SEM). Furthermore, the presence of non-metallic inclusions, such as oxides formed during corrosion processes, causes cracks, further increasing the brittleness of the steel.
- The results obtained in the conducted research confirm the findings from [17, 20, 32]. In these publications, the decreases in material parameters were given depending on the percentage of corrosion, and not as a function of ion concentration, which is not practical for the structure diagnostics. The introduced functions for changes in the mechanical parameters of the internal steel reinforcement based on the concentration of chloride ions c_{Cl}, are a much more convenient form of estimating material degradation. Furthermore, the proposed linear trend lines are to be replaced in future studies with much more accurate non-linear models, which is the next stage of research and development of the proposed methodology. Direct measurement of chloride ion concentration, followed by reference to the proposed dependence functions (Figure 10), can be particularly helpful when estimating element stiffness (e.g., for the analysis of deflections or structural deformations). Similar behavior is assumed for steels of other diameters, but direct translation of results to other diameters without further testing is not recommended.
- Changes in the parameters of the steel bars depend on the concentration of the aggressive factor (Cl^- ions) and the presence of concrete cover. In the case of changes in the yield strength, the maximum decrease (28.63 %) was obtained in an environment with a concentration of 6 % NaCl for elements without cover. Similarly, for the same conditions, a reduction in the ultimate tensile strength of 32.06 % was achieved. Elastic modulus also strongly depends on the concentration of chloride ions and the presence of concrete cover. The maximum reduction in elastic modulus was obtained for samples without concrete cover in a 6 % chlorine ion concentration and reached up to 10.77 % of the initial value. The resulting changes were caused by the breakdown of the passive oxide layer, which protects the reinforcement surface from initiating corrosion processes. The obtained test results confirm the proportional relationship between the increase in aggressive factors and the reduction in the protective properties of the concrete cover, and the progressive damage and changes in the mechanical parameters of the reinforcement.

– Presented research confirms the significant impact of concrete cover for the internal steel reinforcement, which prevents the progress of the mechanical properties degradation due to limited access of oxygen and moisture. Consequently, limiting the development of electrode processes on the surface of the steel reinforcement. The test results showed that, in the absence of a concrete cover, changes in the yield strength of the steel bars are much greater than in the case when the bars are protected with a tight layer of concrete cover. Otherwise, it is therefore necessary to use other tight means of protection against the inflow of chloride ions e.g. [42–44].

Acknowledgments: The authors are grateful for the financial support received from the Academy of Silesia in Katowice (Poland).

Data Availability Statement: All data, models, and code generated or used during the study appear in the submitted article.

Conflict of interest: No conflict of interest exits in the submission of this manuscript, which is approved by all authors for publication.

Author contributions statement: conceptualization, F.R.; data curation, F.R. and K.Ł.; formal analysis, F.R.; funding acquisition, F.R. and K.Ł.; investigation, F.R.; methodology, F.R.; project administration, F.R.; resources, F.R, M.J.J. and T.K.; software, F.R.; supervision, F.R., and T.K.; validation, F.R., K.Ł., M.J.J. and T.K.; visualization, F.R.; writing—original draft preparation, F.R, K.Ł.; writing—review and editing, M.J.J. and T.K. All authors have read and agreed to the published version of the manuscript.

Funding information: This research received no external funding.

References

1. Arredondo-Rea SP, Corral-Higuera R, Gómez-Soberón JM, Gámez-García DC, Bernal-Camacho JM, Rosas-Casarez CA, et al. Durability parameters of reinforced recycled aggregate concrete: case study. Appl Sci 2019;9:617.
2. Bazant ZP. Physical model for steel corrosion in concrete sea structures —theory. J Struct Div 1979;105:1137–53. ASCE.
3. Xi Y, Bazant ZP. Modeling chloride penetration in saturated concrete. J Mater Civ Eng 1999;11:58–65.
4. Tang Bui H, Maekawa K, Hai Tan K. Analytical model of corrosion-induced cracks in concrete considering time-varying deformations of layers, mechanical properties of rust. Constr Build Mater 2022;316: 125883.
5. Maekawa K, Ishida T, Kishi T. Multi-scale modeling of concrete performance. J Adv Concr Technol 2003;1:91–126.
6. Nicolás AF, Menchaca Campos EC, Nicolás MF, Gonzalez Noriega OA, García Peréz CA, Chavarín JU. Corrosion resistance of reinforcing steel in concrete using natural fibers treated with used engine oil. Civ Eng J (Iran) 2024;10:1012–33.
7. Černý R, Rovnaníková P. Transport processes in concrete. London; New York: CRC Press; 2002:275–332 pp.
8. Caijun S, Qiang Y, Fuqiang H, Xiang H. Transport and interactions of chlorides in cement-based materials. London: CRC Press; 2019.
9. Michel A, Pease BJ, Peterová A, Geiker MR, Stang H, Thybo AEA. Penetration of corrosion products and corrosion-induced cracking in reinforced cementitious materials: experimental investigations and numerical simulations. Cem Concr Compos [Internet] 2014;47:75–86. Available from.
10. Krykowski T, Jaśniok T, Recha F, Karolak M. A cracking model for reinforced concrete cover, taking account of the accumulation of corrosion products in the ITZ layer, and including computational and experimental verification. Materials 2020;13:5375.
11. Šavija B, Luković M, Pacheco J, Schlangen E. Cracking of the concrete cover due to reinforcement corrosion: a two-dimensional lattice model study. Constr Build Mater 2013;44:626–38.
12. Jamshidi F, Dehestani M. Time to cracking in concrete cover length due to reinforcement corrosion via a simplified fracture mechanics approach. Constr Build Mater [Internet] 2020;258:119588. Available from.
13. Chen J, Zhang W, Tang Z, Huang Q. Experimental and numerical investigation of chloride-induced reinforcement corrosion and mortar cover cracking. Cem Concr Compos [Internet] 2020;111:103620. Available from.
14. Capozucca R. Damage to reinforced concrete due to reinforcement corrosion. Constr Build Mater 1995;9:295–303.
15. Fischer C. Auswirkungen der Bewehrungskorrosion auf den Verbund zwischen Stahl und Beton. Stuttgart, Germany: Institut für Werkstoffe im Bauwesen der Universität Stuttgart; 2012.
16. El AE, Fekak FE, Garibaldi L, Moustabchir H, Elkhalfi A, Scutaru ML, et al. Numerical study of the bond strength evolution of corroded reinforcement in concrete in pull-out tests. Appl Sci 2022;12:654.
17. Lee HS, Noguchi T, Tomosawa F. Evaluation of the bond properties between concrete and reinforcement as a function of the degree of reinforcement corrosion. Cement Concr Res 2002;32: 1313–8.
18. Almusallam AA. Effect of degree of corrosion on the properties of reinforcing steel bars. Constr Build Mater 2001;15:361–8.
19. Zhou B, Sun X, Zou D, Wang H. Evaluation of corrosion morphology on mechanical properties of reinforcing steel bars using numerical simulation and simplified analytical model. J Build Eng [Internet] 2022; 52:104380. Available from.
20. Moreno E, Cobo A, Palomo G, González MN. Mathematical models to predict the mechanical behavior of reinforcements depending on their degree of corrosion and the diameter of the rebars. Construct Build Mater [Internet] 2014;61:156–63. Available from.
21. Andrade C. Some historical notes on the research in corrosion of reinforcement. Hormigón y Acero 2018;69:21–8.
22. Benjamin I, Kennedy C, Wurah IF. Effects of corrosion on mechanical properties of reinforcing steel residual flexural strength. Abbreviated key title. Sch Int J Chem Mater Sci [Internet] 2021;4:158–73. Available from: http://saudijournals.com.
23. Negrutiu C, Sosa IP, Constantinescu H, Heghes B. Crack analysis of reinforced high strength concrete elements in simulated aggressive environments. Proced Technol [Internet] 2016;22:4–12. Available from.
24. Shen J, Gao X, Li B, Du K, Jin R, Chen W, et al. Damage evolution of RC beams under simultaneous reinforcement corrosion and sustained load. Materials 2019;12:1–16.

25. Recha F. Estimation method of corrosion current density of RC elements. Open Eng 2023;13:20220430.
26. Grandić D, Bjegović D, IŠ G. Deflection of reinforced concrete beams simultaneously subjected to sustained load and reinforcement corrosion. In: Structural Engineers World Congress 2011. Como, Italy: SEWC; 2011.
27. Jin X, Tong J, Tian Y, Jin N. Time-varying relative displacement field on the surface of concrete cover caused by reinforcement corrosion based on DIC measurement. Construct Build Mater [Internet] 2018;159: 695–703. Available from.
28. Ye H, Fu C, Jin N, Jin X. Performance of reinforced concrete beams corroded under sustained service loads: a comparative study of two accelerated corrosion techniques. Construct Build Mater [Internet] 2018;162:286–97. Available from.
29. De Sitter. CEB-RILEM Workshop Report. Durability of concrete structures. CEB-Bulletin. Kopenhaga; 1983:1983 p.
30. Li L, Mahmoodian M, Khaloo A, Sun Z. Risk-cost optimized maintenance strategy for steel bridge subjected to deterioration. Sustainability 2022; 14:436.
31. Zhu W, François R, Poon CS, Dai JG. Influences of corrosion degree and corrosion morphology on the ductility of steel reinforcement. Constr Build Mater 2017;148:297–306.
32. Lee HS, Cho YS. Evaluation of the mechanical properties of steel reinforcement embedded in concrete specimen as a function of the degree of reinforcement corrosion. Int J Fract 2009;157:81–8.
33. Chen Z, Nie S, Han W, Tang M, Yang B, Elchalakani M. A study on static properties of high-performance steel after corrosion damage. J Constr Steel Res [Internet] 2023;207:107970. Available from.
34. Polish Committee of Normalization. Norm PN-EN 1992-1-1 eurocode 2: design of concrete structures. Part 1-1: general rules and regulations for buildings. Warsaw: Polish Committee of Normalization; 2008.
35. PN-EN ISO 6892 Metals. Tensile test. In: Room temperature test method. Warsaw: Polish Committee of Normalization; 2010.
36. Chen E, Berrocal CG, Fernandez I, Löfgren I, Lundgren K. Assessment of the mechanical behaviour of reinforcement bars with localised pitting corrosion by digital image correlation. Eng Struct [Internet] 2020;219: 110936. Available from.
37. Tutti K. Corrosion of steel in concrete. Stockholm: Swedish Cement and Concrete Research Institute; 1982.
38. Yu L, François R, Dang VH, L'Hostis V, Gagné R. Distribution of corrosion and pitting factor of steel in corroded RC beams. Construct Build Mater [Internet] 2015;95:384–92. Available from.
39. Stewart MG, Al-Harthy A. Pitting corrosion and structural reliability of corroding RC structures: experimental data and probabilistic analysis. Reliab Eng Syst Saf 2008;93:373–82.
40. Val DV, Trapper PA. Probabilistic evaluation of initiation time of chloride-induced corrosion. Reliab Eng Syst Saf 2008;93:364–72.
41. Castaneda H, Okeil AM. Technology O of the AS for R and, (Tran-SET) TC of S-CS. Corros Manag Syst Regional Reinf Concr (RC) Bridges 2020;19: 97p.
42. Hsissou R, Benzidia B, Hajjaji N, Elharfi A. Elaboration and electrochemical studies of the coating behavior of a new pentafunctional epoxy polymer (pentaglycidyl ether pentabisphenol phosphorus) on E24 carbon steel in 3.5 % NaCl. J Chem Technol Metall 2018;53:898–905.
43. Molhi A, Hsissou R, Damej M, Berisha A, Bamaarouf M, Seydou M, et al. Performance of two epoxy compounds against corrosion of C38 steel in 1 M HCl: electrochemical, thermodynamic and theoretical assessment. Int J Corros Scale Inhib 2021;10:812–37.
44. Hsissou R, Lachhab R, El Magri A, Echihi S, Vanaei HR, Galai M, et al. Synthesis characterization and highly protective efficiency of tetraglycidyloxy pentanal epoxy prepolymer as a potential corrosion inhibitor for mild steel in 1 M HCl medium. Polymers 2022;14:1–14.